NSS

Neutrosophic Sets and Systems, Vol. 97, 2026

University of New Mexico

Entropy Generation in EMHD Hybrid Nanofluids: A Neutrosophic Approach with Thermal Radiation and Melting Effects

Srinivasan J[1], Balakrishnan S[2*], Kanchana M[3].

[1] PG and Research Department of Mathematics, Islamiah College(Autonomous), (Affiliated to Thiruvalluvar University, Serkkadu, Vellore 632 115, Tamilnadu, India), Vaniyambadi 635 752, Tamilnadu, India; vjsrivas23@gmail.com

[3]Kingston Engineering College, Vellore, India; mkanchana378@gmail.com

[2*]Correspondence:PG and Research Department of Mathematics, Islamiah College(Autonomous), (Affiliated to Thiruvalluvar University, Serkkadu, Vellore 632 115, Tamilnadu, India), Vaniyambadi 635 752, Tamilnadu, India.

sma4maths@gmail.com;

Abstract. Entropy generation in hybrid nanofluid flows under electromagnetic and thermal effects is crucial for enhancing energy efficiency in advanced engineering systems. This study focuses on the steady electromagneto-hydrodynamic (EMHD) stagnation point flow of a Cu–Al_2O_3/water hybrid nanofluid over a stretching surface, taking into account the roles of thermal radiation and surface melting. To effectively capture uncertainties arising from fluctuating thermal properties and boundary conditions, a neutrosophic approach is adopted. The governing partial differential equations are transformed into Neutrosophic Differential Equations (NDEs), integrating degrees of truth, indeterminacy, and falsity. These equations are numerically solved using a fourth-order Runge–Kutta method in combination with a shooting technique.

The analysis examines how key physical and neutrosophic parameters influence the velocity field, temperature distribution, entropy generation, and Bejan number. Comparative assessments with classical deterministic and Homotopy Perturbation Method (HPM) models confirm the improved adaptability and robustness of the neutrosophic framework. Additionally, sensitivity analysis underscores the model's effectiveness in handling parameter uncertainty.

The results provide valuable insights for optimizing heat transfer systems in contexts where precise data may be unavailable, with applications ranging from microscale cooling devices to industrial thermal processes. The study also outlines model limitations and directions for future research.

Keywords: EMHD Hybrid Nanofluid; Entropy Generation; Neutrosophic Uncertainty; Numerical Simulation; Heat Transfer.

AMS Subject Classification: 76W05, 76D10, 80A20, 94A17.

1. Introduction

The study of nanofluid heat transfer has become fundamental to thermal engineering research. One of the earliest and most recognized models is the convective transport framework proposed by Buongiorno [1], which explains enhancement in thermal conductivity due to Brownian motion and thermophoresis effects.

Abelman [2] extended this to incorporate MHD nanofluid flow using a two-phase mixture model, which offers greater realism than single-phase models by accounting for nanoparticle interactions. Hayat et al. [3] investigated MHD stagnation point flow of hybrid nanofluids over a stretching sheet, emphasizing the role of convective boundary conditions on heat transfer efficiency. Chamkha et al. [4] presented entropy generation in MHD nanofluid flow within porous enclosures and underlined the importance of magnetic field effects in optimizing entropy generation.

Smarandache [5] introduced neutrosophic sets, extending fuzzy logic to better represent uncertainty, laying the theoretical groundwork for applying such logic in fluid dynamics. Nadeem and Ijaz [6] analyzed MHD nanofluid flow with chemical reaction effects, showing its influence on entropy generation. Rashidi et al. [7] conducted a detailed entropy analysis considering conduction and convection effects.

Khan et al. [8] compared Cu, Ag, and Al_2O_3 nanoparticles in EMHD hybrid nanofluids and demonstrated their relative thermal performance. Liu and Zhang [9] numerically examined entropy generation in hybrid nanofluid flow and investigated the impact of nonlinear stretching sheets. Kumari and Hussain [10] studied entropy generation under variable thermal conductivity conditions.

Kayalvizhi and Vijayakumar [11] incorporated entropy generation in EMHD hybrid nanofluid stagnation point flow with melting effects, validating MATLAB solutions against HPM. Daniel [12] studied entropy generation in electrically driven MHD nanofluid flow under combined thermal radiation and chemical reaction influences.

Recent works also investigated entropy generation in more complex geometries and heating conditions, such as in a wavy cavity [13], under variable magnetic fields [14], or in 3D flows over variable-thickness surfaces [15]. These studies contribute to modeling improvements but often rely on deterministic assumptions.

Traditional models generally neglect the role of uncertainty in boundary conditions, thermophysical properties, and flow variations. While fuzzy logic and probabilistic approaches have been used, neutrosophic logic allows a more general framework by accounting for degrees of truth, indeterminacy, and falsity simultaneously.

This study addresses the existing gap by applying neutrosophic logic to the modeling of entropy generation in EMHD hybrid nanofluid stagnation point flow, including thermal radiation and melting effects. By reformulating the governing equations as Neutrosophic Differential Equations (NDEs), the study aims to enhance the realism and flexibility of entropy prediction under uncertain conditions.

1.1. *Motivation and Novel Contributions*

Entropy generation plays a central role in determining the performance and irreversibility of thermal systems, especially in high-efficiency applications such as micro-electromechanical systems (MEMS), solar energy collectors, and cooling technologies in aerospace and biomedical devices ([6, 9]). The analysis of entropy in such systems becomes more critical when hybrid nanofluids and electromagnetic fields are involved, as they introduce nonlinear effects and parameter sensitivities ([8, 11]).

While classical models based on deterministic approaches have been extensively used to study magnetohydrodynamic (MHD) and nanofluid flows ([1, 3, 4]), they often fail to accommodate uncertainties in input data, including material properties, boundary conditions, and external forcing. These uncertainties are particularly relevant in real-world scenarios, where experimental or operational variability can influence heat transfer rates and entropy production.

To overcome these challenges, this work introduces a Neutrosophic Differential Equation (NDE) framework for modeling electromagnetohydrodynamic (EMHD) hybrid nanofluid flows over a stretching surface [5]. By incorporating the triple components of truth, indeterminacy, and falsity, the neutrosophic model offers a more flexible and realistic approach to uncertainty representation than conventional fuzzy or interval methods.

The core contributions of this study are as follows:

- Development of a neutrosophic formulation for EMHD hybrid nanofluid flow, integrating the effects of thermal radiation and surface melting.
- Reformulation of governing equations using neutrosophic logic, allowing uncertainty to be embedded directly into the mathematical structure.
- Implementation of a fourth-order Runge–Kutta method coupled with a shooting technique for solving the neutrosophic equations.
- Comprehensive analysis of the impact of neutrosophic parameters on entropy generation, velocity, temperature, and Bejan number.
- Validation of the proposed model through comparative results with crisp solutions and the Homotopy Perturbation Method (HPM) [11].

- Inclusion of sensitivity analysis to quantify the effects of neutrosophic uncertainty on entropy behavior.

This framework provides enhanced adaptability for modeling thermofluid systems under uncertain operating conditions, contributing both theoretically and computationally to the field of thermal sciences.

1.2. *Literature Review*

Numerous studies have been conducted to examine the behavior of hybrid nanofluids in the presence of electromagnetic effects, radiation, and entropy generation. Buongiorno [1] introduced a two-phase model for nanofluid convection considering Brownian motion and thermophoresis. Abelman [2] extended this to MHD flows using a two-phase mixture model.

Hayat et al. [3] analyzed stagnation point flow of hybrid nanofluids over stretching surfaces under convective boundary conditions. Chamkha et al. [4] explored MHD nanofluid behavior in porous media and emphasized entropy generation analysis. These studies largely adopted deterministic approaches, assuming fixed thermophysical parameters.

Rashidi et al. [7] and Khan et al. [8] emphasized entropy generation in hybrid nanofluids under magnetic field influence. Nadeem and Ijaz [6] explored chemical reaction effects on MHD nanofluid flow, while Liu and Zhang [9] examined entropy generation in flow over nonlinear stretching surfaces. Kumari and Hussain [10] considered variable thermal conductivity impacts.

Daniel et al. [12] investigated combined effects of thermal radiation and electric fields on entropy generation in nanofluids, highlighting the role of external forces. Kayalvizhi and Vijayakumar [11] studied EMHD hybrid nanofluid flows with melting effects and validated their findings using MATLAB and HPM solutions.

In recent years, several studies have extended entropy generation analysis to more complex domains. For instance, Ibrahim [32] considered magnetized hybrid nanofluid flow in a wavy enclosure with heat generation and thermal radiation. Al-Kouz et al. [33] examined heat transfer and entropy generation in a trapezoidal enclosure filled with water–Fe_3O_4/CNT hybrid magnetic nanofluid. Mebarek-Oudina et al. [34] analyzed the role of porous structures in magneto-convective hybrid nanofluid systems. Murugan et al. [35] incorporated thermo-radiative and ohmic dissipation effects on hybrid nanofluid motion. More recently, Shateri et al. [36] studied entropy behavior in star-shaped porous cavities with magnetic field inclination and hybrid nanofluid flow.

Despite the comprehensive nature of these models, most adopt crisp parameter values and deterministic boundary conditions, overlooking the inherent uncertainties in real-world

systems. Fluctuations in nanoparticle distribution, material properties, and magnetic field strength can significantly influence entropy generation predictions.

To address this research gap, the present study employs neutrosophic logic, originally proposed by Smarandache [5], to embed uncertainty directly into the governing equations. This approach enables modeling of truth, indeterminacy, and falsity within a unified differential equation framework.

Thus, this review establishes both the relevance and the novelty of applying neutrosophic modeling to entropy generation analysis in EMHD hybrid nanofluid flow with radiation and melting effects.

2. **Methodology**

2.1. *Overview of the Modelling Strategy*

Flow chart summarises the workflow adopted in this study. The key stages are:

(1) **Parameter Definition:** Specify the thermophysical properties of the Cu–Al_2O_3/water hybrid nanofluid, electromagnetic field strengths, and boundary conditions (see Table 2 of the [11]).

(2) **Classical Governing Equations:** Begin with the steady, laminar EMHD stagnation-point momentum and energy equations, including viscous dissipation, thermal radiation, and surface melting terms (Eqs. (1)–(2) [11]).

(3) **Neutrosophic Reformulation:** Replace each crisp variable and parameter by its neutrosophic counterpart, e.g. $u \to u^{\mathcal{N}} = (T_u, I_u, F_u)$, to obtain the Neutrosophic Differential Equations (NDEs) given in Eqs. (3)–(4).

(4) **Similarity Transformations:** Apply the transformations in Eq. (23) to reduce the NDEs to coupled ordinary differential equations (ODEs) with neutrosophic coefficients (Eqs. (24)–(25)).

(5) **Numerical Scheme:**
   (a) Discretise the domain $0 \le \eta \le \eta_\infty$.
   (b) Convert the 3rd- and 2nd-order ODEs to a first-order system (Eq. (S)) by introducing the state vector $\mathbf{S}^{\mathcal{N}} = [f^{\mathcal{N}}, f^{\mathcal{N}\prime}, f^{\mathcal{N}\prime\prime}, \theta^{\mathcal{N}}, \theta^{\mathcal{N}\prime}]^\top$.

(6) **Shooting Method:** Guess the missing initial slopes $f^{\mathcal{N}\prime}(0)$ and $\theta^{\mathcal{N}\prime}(0)$, integrate the ODE system with a 4th-order Runge–Kutta routine, and iteratively update the guesses via a Newton–Raphson loop until the far-field conditions $f^{\mathcal{N}\prime}(\eta_\infty) \to 1$ and $\theta^{\mathcal{N}}(\eta_\infty) \to 1$ are met (tolerance 10^{-6}).

(7) **Post-Processing:** Compute skin-friction, Nusselt number, entropy generation $NG^{\mathcal{N}}$, and Bejan number $Be^{\mathcal{N}}$; validate against crisp and HPM solutions; perform parameter sweeps and sensitivity analysis.

2.2. *Algorithmic Flowchart*

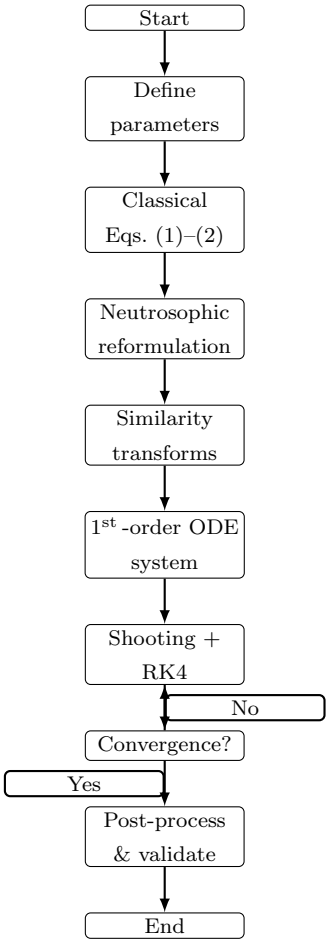

FIGURE 1. Algorithmic flowchart for the neutrosophic EMHD hybrid nanofluid model.

Figure 1 outlines the complete numerical procedure followed in this study. It begins with the definition of hybrid nanofluid parameters and governing equations, which are reformulated using neutrosophic logic to account for uncertainty. The resulting Neutrosophic Differential Equations (NDEs) are simplified through similarity transformations and solved numerically using a fourth-order Runge-Kutta method coupled with a shooting technique. The process continues until convergence is achieved, after which entropy generation and Bejan number results are computed and analyzed.

3. Mathematical Preliminaries

In classical fluid dynamics, the governing equations assume deterministic behavior with known physical properties and boundary conditions. However, in many real-world scenarios, parameters such as surface temperature, viscosity, or magnetic field strength are not precisely measurable due to experimental variability and environmental fluctuations. To address such uncertainty, this study incorporates the neutrosophic framework.

3.1. *Neutrosophic Numbers and Functions*

Let $x^{\mathcal{N}}$ denote a Neutrosophic number defined as:

$$x^{\mathcal{N}} = (\mathscr{T}(x), \mathscr{I}(x), \mathscr{F}(x)),$$

where $\mathscr{T}(x)$, $\mathscr{I}(x)$, and $\mathscr{F}(x) \in [0, 1]$ represent the degrees of truth, indeterminacy, and falsity associated with the quantity x.

A Neutrosophic function $f^{\mathcal{N}}(x^{\mathcal{N}})$ transforms a Neutrosophic input into a corresponding Neutrosophic output:

$$f^{\mathcal{N}}(x^{\mathcal{N}}) = (\mathscr{T}(f(x)), \mathscr{I}(f(x)), \mathscr{F}(f(x))).$$

This representation extends beyond classical and fuzzy logic by explicitly modeling ambiguity, partial ignorance, and conflicting information within a unified mathematical structure.

3.2. *Extension to Governing Equations*

In a classical model, variables such as fluid velocity u, temperature T, and entropy generation S are treated as deterministic functions governed by partial differential equations. In the Neutrosophic approach, these variables are reformulated as:

$$u^{\mathcal{N}} = (\mathscr{T}_u, \mathscr{I}_u, \mathscr{F}_u), \quad T^{\mathcal{N}} = (\mathscr{T}_T, \mathscr{I}_T, \mathscr{F}_T), \quad S^{\mathcal{N}} = (\mathscr{T}_S, \mathscr{I}_S, \mathscr{F}_S).$$

These neutrosophic variables capture both the expected behavior and the range of uncertainty surrounding each physical quantity. For instance, the momentum equation becomes:

$$\frac{du^{\mathcal{N}}}{dy} = f^{\mathcal{N}}\left(u^{\mathcal{N}}, T^{\mathcal{N}}, M^{\mathcal{N}}, \dots\right),$$

where $M^{\mathcal{N}}$ is the Neutrosophic magnetic parameter. Each component in the equation reflects not only its nominal value but also its degree of uncertainty.

3.3. *Treatment of Neutrosophic Parameters*

To simulate uncertain parameters numerically, we use bounded intervals derived from the truth and indeterminacy parts. For example, the Neutrosophic viscosity ratio $\varepsilon^{\mathcal{N}} = (\mathscr{T}_\varepsilon, \mathscr{I}_\varepsilon, \mathscr{F}_\varepsilon)$ is approximated by:

$$\varepsilon^{\text{lower}} = \mathscr{T}_\varepsilon - \mathscr{I}_\varepsilon, \quad \varepsilon^{\text{upper}} = \mathscr{T}_\varepsilon + \mathscr{I}_\varepsilon.$$

This bracketed range allows the system to be evaluated under best-case and worst-case assumptions, producing a behavioral envelope rather than a single outcome.

3.4. *Reduction to Classical Case*

When the indeterminacy vanishes, i.e., $\mathscr{I}(x) = 0$, and the falsity satisfies $\mathscr{F}(x) = 1 - \mathscr{T}(x)$, the Neutrosophic expression simplifies to:

$$x^{\mathcal{N}} \to x.$$

Thus, the classical deterministic model is recovered as a special case of the general Neutrosophic formulation, ensuring theoretical consistency and compatibility.

4. **Neutrosophic Mathematical Modeling**

This section describes the mathematical formulation of EMHD hybrid nanofluid flow over a stretching surface with thermal radiation and melting effects, and its extension into the Neutrosophic framework.

4.1. *Classical Formulation*

The dimensionless momentum and energy equations, assuming laminar and steady flow, are given by:

$$f''' + ff'' - f'^2 - Mf' = 0, \tag{1}$$

$$\theta'' + Pr f\theta' + Ec\, Pr\, f''^2 - R\theta + \delta_m\theta = 0, \tag{2}$$

Here, f is the non-dimensional stream function, θ is the non-dimensional temperature, and M, Pr, Ec, R, and δ_m represent the magnetic field parameter, Prandtl number, Eckert number, radiation parameter, and melting coefficient, respectively.

The entropy generation number $\mathcal{N}_s$ and the Bejan number Be are given by:

$$\mathcal{N}_s = \frac{k(T_w - T_\infty)^2}{\mu u_0^2}\left(f''^2 + \gamma\,\theta'^2\right), \quad Be = \frac{\gamma\,\theta'^2}{f''^2 + \gamma\,\theta'^2},$$

where γ quantifies the relative weight of heat transfer irreversibility. These classical expressions provide the basis for subsequent Neutrosophic extension.

4.2. *Neutrosophic Reformulation*

To incorporate parametric uncertainty, we extend the classical system using Neutrosophic logic. Each parameter α is replaced with a Neutrosophic counterpart $\alpha^{\mathcal{N}} = (\mathscr{T}_\alpha, \mathscr{I}_\alpha, \mathscr{F}_\alpha)$, and the dependent variables are represented as Neutrosophic-valued functions:

$$f^{\mathcal{N}}(\eta) = (\mathscr{T}_f, \mathscr{I}_f, \mathscr{F}_f), \quad \theta^{\mathcal{N}}(\eta) = (\mathscr{T}_\theta, \mathscr{I}_\theta, \mathscr{F}_\theta).$$

The reformulated Neutrosophic momentum and energy equations take the form:

$$(f^{\mathcal{N}})''' + f^{\mathcal{N}}(f^{\mathcal{N}})'' - ((f^{\mathcal{N}})')^2 - M^{\mathcal{N}}(f^{\mathcal{N}})' = 0, \tag{3}$$

$$(\theta^{\mathcal{N}})'' + Pr^{\mathcal{N}} f^{\mathcal{N}}(\theta^{\mathcal{N}})' + Ec^{\mathcal{N}} Pr^{\mathcal{N}}((f^{\mathcal{N}})'')^2 - R^{\mathcal{N}}\theta^{\mathcal{N}} + \delta_m^{\mathcal{N}}\theta^{\mathcal{N}} = 0. \tag{4}$$

Similarly, the entropy generation and Bejan number under neutrosophic uncertainty are:

$$\mathcal{N}_s^{\mathcal{N}} = \left(f^{\mathcal{N}''}\right)^2 + \gamma^{\mathcal{N}}\left(\theta^{\mathcal{N}'}\right)^2, \quad Be^{\mathcal{N}} = \frac{\gamma^{\mathcal{N}}\left(\theta^{\mathcal{N}'}\right)^2}{\left(f^{\mathcal{N}''}\right)^2 + \gamma^{\mathcal{N}}\left(\theta^{\mathcal{N}'}\right)^2}.$$

These coupled equations are solved using a fourth-order Runge–Kutta shooting technique, with simulations performed across the lower and upper neutrosophic bounds for each parameter.

5. **Neutrosophic Mathematical Formation of EMHD**

The physical model considers a steady, incompressible, two-dimensional, electrically conducting hybrid nanofluid over a stretching sheet embedded in a porous medium, under the influence of a magnetic field, thermal radiation, melting effects, and viscous dissipation. Neutrosophic Logic is applied to model uncertainty via three membership values: truth ($\mathscr{T}$), indeterminacy ($\mathscr{I}$), and falsity ($\mathscr{F}$).

The velocity field at the wall and free stream are expressed as $u_w(x) = cx$ and $u_e(x) = \omega x$, respectively. Their Neutrosophic representations are described as:

- $\mathscr{T}_u$: Accurate modeling under known boundary conditions.
- $\mathscr{I}_u$: Uncertainty due to slip, roughness, or other physical variations.
- $\mathscr{F}_u$: Simplified assumptions such as neglecting micro-scale turbulence.

Electromagnetic Effects: The flow obeys Maxwell's equations and Ohm's law in the presence of electric and magnetic fields:

$$\mathbf{J} = \sigma(\mathbf{E} + \mathbf{v} \times \mathbf{B}),$$

where σ is electrical conductivity, $\mathbf{v}$ is fluid velocity, and $\mathbf{J}$ is current density.

- $\mathscr{T}_B$: The magnetic field's effect on velocity and temperature is captured as expected.
- $\mathscr{I}_B$: Uncertainty arises from variable conductivity and field intensity.
- $\mathscr{F}_B$: Simplifications include neglecting induced fields or assuming magnetic uniformity.

- $\mathscr{T}_J$: The law captures current density in magnetohydrodynamic flows.
- $\mathscr{I}_J$: Indeterminacy from conductivity variations or perturbations.
- $\mathscr{F}_J$: Ignoring dynamic redistribution of charges.

Thermal Effects and Melting: The temperature boundary condition involves a melting temperature T_m and far-field temperature T_∞, with $T_m < T_\infty$.

- $\mathscr{T}_T$: Well-established conduction and radiation terms.
- $\mathscr{I}_T$: Effects like anisotropic radiation and variable nanofluid properties.
- $\mathscr{F}_T$: Assuming constant thermal conductivity or ignoring temperature-dependent viscosity.

Entropy Generation in Neutrosophic Context: Entropy production from viscous, thermal, and electromagnetic irreversibilities is modeled via:

$$S^{\mathcal{N}} = \mathscr{T}_S S + \mathscr{I}_S S + \mathscr{F}_S S,$$

where:

- $\mathscr{T}_S S$: Represents true entropy due to physical mechanisms.
- $\mathscr{I}_S S$: Captures entropy due to uncertain effects like material inconsistencies.
- $\mathscr{F}_S S$: Includes neglected or misrepresented sources such as thermoelectric loss.

Following the neutrosophic formulation in [15–17], the continuity equation remains unchanged:

$$\frac{\partial u}{\partial x} + \frac{\partial v}{\partial y} = 0.$$

The momentum equation, incorporating Neutrosophic viscosity, density, conductivity, and permeability, becomes:

$$u\frac{\partial u}{\partial x} + v\frac{\partial v}{\partial y} = u_e\frac{du_e}{dx} + \frac{\mu_{hnf}^{(\mathcal{N})}}{\rho_{hnf}^{(\mathcal{N})}}\frac{\partial^2 u}{\partial y^2} + \frac{\sigma_{hnf}^{(\mathcal{N})}}{\rho_{hnf}^{(\mathcal{N})}}\left[E_0 B_0 - B_0^2(u_e - u)\right] - \frac{\mu_{hnf}^{(\mathcal{N})}}{\rho_{hnf}^{(\mathcal{N})}}\frac{1}{K^{(\mathcal{N})}}(u_e - u). \tag{5}$$

Uncertainty Considerations in Hybrid Nanofluid Flow:

In real-world thermal systems, physical parameters rarely remain fixed due to environmental variability, manufacturing tolerances, or measurement errors. To model these uncertainties, the governing equations are extended using neutrosophic logic, which associates each quantity with three components: truth ($\mathscr{T}$), indeterminacy ($\mathscr{I}$), and falsity ($\mathscr{F}$). Parameters such as dynamic viscosity $\mu_{hnf}^{(\mathcal{N})}$, density $\rho_{hnf}^{(\mathcal{N})}$, electrical conductivity $\sigma_{hnf}^{(\mathcal{N})}$, and permeability $K^{(\mathcal{N})}$ are modeled as follows:

- $\mathscr{T}$: True component based on known or measured data.
- $\mathscr{I}$: Indeterminate component capturing fluctuations and experimental uncertainty.

- $\mathscr{F}$: Falsity component representing simplifications or unrealistic assumptions.

This approach allows the model to incorporate realistic deviations in nanofluid behavior and enhances the robustness of entropy and heat transfer predictions.

Boundary Conditions under Neutrosophic Logic:

The classical melting surface condition as given by Roberts [19] is:

$$k_{hnf}^{(\mathscr{N})}\left(\frac{\partial T}{\partial y}\right)_{y=0} = \rho_{hnf}^{(\mathscr{N})}\left[c_s(T_m - T_0) + L\right] v(x,0) \tag{6}$$

The slip velocity condition from Lin Wu [20] reads:

$$u_{\text{slip}} = \lambda^{(\mathscr{N})}\frac{\partial u}{\partial y} + \mu_{\text{slip}}^{(\mathscr{N})}\frac{\partial^2 u}{\partial y^2} \tag{7}$$

Rewriting these classical expressions with neutrosophic parameters leads to:

$$u = u_{\text{slip}} + u_w(x), \quad T_m = T^{(\mathscr{N})} \tag{8}$$

$$T \to T_\infty^{(\mathscr{N})}, \quad u \to u_e^{(\mathscr{N})}(x), \quad y \to \infty \tag{9}$$

$$k_{hnf}^{(\mathscr{N})}\left(\frac{\partial T}{\partial y}\right)_{y=0} = \rho_{hnf}^{(\mathscr{N})}\left[c_s(T_m - T_0) + L\right] v(x,0) \tag{10}$$

$$u_{\text{slip}} = \lambda^{(\mathscr{N})}\frac{\partial u}{\partial y} + \mu_{\text{slip}}^{(\mathscr{N})}\frac{\partial^2 u}{\partial y^2} \tag{11}$$

- $T^{(\mathscr{N})}$: Neutrosophic form of temperature.
- $u_e^{(\mathscr{N})}(x)$: Flow velocity with uncertain influences.
- $k_{hnf}^{(\mathscr{N})}$: Thermal conductivity incorporating uncertainty.

Thermophysical Property Modeling under Uncertainty: [18]

Neutrosophic forms of key thermophysical properties used in this study are:

Thermal Conductivity:

$$\frac{k_{hnf}^{(\mathscr{N})}}{k_f} = \frac{2(1-\phi)k_f + (1+2\phi_1)k_{1s} + (1+2\phi_2)k_{2s}}{(2-\phi)k_f + (1-\phi_1)k_{1s} + (1-\phi_2)k_{2s}} \tag{12}$$

Dynamic Viscosity:

$$\frac{\mu_{hnf}^{(\mathscr{N})}}{\mu_f} = (1-\phi)^{-2.5} \tag{13}$$

Density:

$$\frac{\rho_{hnf}^{(\mathscr{N})}}{\rho_f} = (1-\phi) + \frac{\phi_1\rho_{1s}}{\rho_f} + \frac{\phi_2\rho_{2s}}{\rho_f} \tag{14}$$

Heat Capacity:

$$\frac{(\rho c_p)_{hnf}^{(\mathscr{N})}}{(\rho c_p)_f} = (1-\phi) + \phi_1\frac{(\rho c_p)_{1s}}{(\rho c_p)_f} + \phi_2\frac{(\rho c_p)_{2s}}{(\rho c_p)_f} \tag{15}$$

Electrical Conductivity:

$$\frac{\sigma_{hnf}^{(\mathcal{N})}}{\sigma_f} = \frac{1 + 3\sigma_1\sigma_f\phi_1 + \sigma_2\sigma_f\phi_2 - 3\phi\sigma_f}{\sigma_1(1-\phi_1) + \sigma_2(1-\phi_2) + (2+\phi)\sigma_f} \tag{16}$$

Neutrosophic Form of Radiation Heat Flux:

$$q_r^{(\mathcal{N})} = -\frac{4\sigma^{*(\mathcal{N})}}{3k^{*(\mathcal{N})}}\frac{\partial T^{4(\mathcal{N})}}{\partial z} \tag{17}$$

Applying a binomial approximation near T_∞:

$$T^{4(\mathcal{N})} \approx T_\infty^{4(\mathcal{N})} + 4T_\infty^{3(\mathcal{N})}(T^{(\mathcal{N})} - T_\infty^{(\mathcal{N})}) \tag{18}$$

Thus, the radiative heat flux under neutrosophic approximation becomes:

$$q_r^{(\mathcal{N})} \approx -\frac{4\sigma^{*(\mathcal{N})}}{3k^{*(\mathcal{N})}}\frac{\partial}{\partial z}\left((4T^{(\mathcal{N})} - 3T_\infty^{(\mathcal{N})})T_\infty^{3(\mathcal{N})}\right) \tag{19}$$

- $\sigma^{*(\mathcal{N})}$: Neutrosophic Stefan–Boltzmann constant.
- $k^{*(\mathcal{N})}$: Neutrosophic Rosseland absorption coefficient.
- $T^{(\mathcal{N})}$: Temperature field under neutrosophic uncertainty.

5.1. *Neutrosophic Energy Equation*

To incorporate the uncertainties in thermophysical properties more effectively, the classical energy equation is reformulated using Neutrosophic logic. This approach allows a comprehensive representation of physical deviations and modeling imperfections. The revised energy equation is expressed as follows:

$$\begin{aligned} u^{(\mathcal{N})}\frac{\partial T^{(\mathcal{N})}}{\partial x} + v^{(\mathcal{N})}\frac{\partial T^{(\mathcal{N})}}{\partial y} =& \frac{k_{hnf}^{(\mathcal{N})}}{(\rho c_p)_{hnf}^{(\mathcal{N})}}\frac{\partial^2 T^{(\mathcal{N})}}{\partial y^2} + \frac{\mu_{hnf}^{(\mathcal{N})}}{(\rho c_p)_{hnf}^{(\mathcal{N})}}\left(\frac{\partial u^{(\mathcal{N})}}{\partial y}\right)^2 \\ &+ \frac{16\left[(\sigma^*)^{(\mathcal{N})}\right]\left[(T_\infty^3)^{(\mathcal{N})}\right]}{3k^{*(\mathcal{N})}(\rho c_p)_{hnf}^{(\mathcal{N})}}\frac{\partial^2 T^{(\mathcal{N})}}{\partial y^2} \\ &+ \frac{\sigma_{hnf}^{(\mathcal{N})}}{(\rho c_p)_{hnf}^{(\mathcal{N})}}(u^{(\mathcal{N})}B_0^{(\mathcal{N})} - E_0^{(\mathcal{N})})^2 + \frac{Q_0^{(\mathcal{N})}}{(\rho c_p)_{hnf}^{(\mathcal{N})}}(T^{(\mathcal{N})} - T_\infty^{(\mathcal{N})}) \end{aligned} \tag{20}$$

Each term is defined by Neutrosophic representations to reflect possible deviations in experimental or practical environments.

5.2. *Neutrosophic Similarity Transformations*

To simplify the partial differential equations into a set of ordinary differential equations, we employ similarity transformations that incorporate Neutrosophic uncertainty:

$$u^{(\mathscr{N})} = w^{(\mathscr{N})} x f'^{(\mathscr{N})}(\eta), \quad v^{(\mathscr{N})} = -\left(\frac{f^{(\mathscr{N})}(\eta)}{\rho^{(\mathscr{N})} w^{(\mathscr{N})} v_f^{(\mathscr{N})}}\right),$$

$$\frac{T^{(\mathscr{N})} - T_m^{(\mathscr{N})}}{T_\infty^{(\mathscr{N})} - T_m^{(\mathscr{N})}} = \theta^{(\mathscr{N})}(\eta), \quad \eta = \frac{y}{(w^{(\mathscr{N})}/v_f^{(\mathscr{N})})^{1/2}} \tag{21}$$

Here, the transformed variables allow a more compact representation of the governing physics under Neutrosophic constraints.

5.3. *Neutrosophic Transformed Ordinary Differential Equations*

By applying the similarity transformations, the governing equations are reduced to the following coupled Neutrosophic ODEs:

$$\frac{A_1^{(\mathscr{N})}}{A_2^{(\mathscr{N})}} f^{(\mathscr{N})'''} + f^{(\mathscr{N})} f^{(\mathscr{N})''} - \left(f^{(\mathscr{N})'}\right)^2 + 1 + \frac{A_3^{(\mathscr{N})}}{A_2^{(\mathscr{N})}} M^{(\mathscr{N})} \left(E^{(\mathscr{N})} - \left[1 - f^{(\mathscr{N})'}\right]\right) + \frac{A_1^{(\mathscr{N})}}{A_2^{(\mathscr{N})}} K^{(\mathscr{N})} \left[1 - f^{(\mathscr{N})'}\right] = 0 \tag{22}$$

$$\frac{A_4^{(\mathscr{N})}}{Pr^{(\mathscr{N})}} \left(A_5^{(\mathscr{N})} + \frac{4}{3} R^{(\mathscr{N})}\right) \theta^{(\mathscr{N})''} + \frac{A_1^{(\mathscr{N})}}{A_4^{(\mathscr{N})}} Ec^{(\mathscr{N})} (f^{(\mathscr{N})''})^2 + f^{(\mathscr{N})} \theta^{(\mathscr{N})'} + \frac{A_3^{(\mathscr{N})}}{A_4^{(\mathscr{N})}} M^{(\mathscr{N})} Ec^{(\mathscr{N})} (f^{(\mathscr{N})'} - E^{(\mathscr{N})})^2 + \frac{Q^{(\mathscr{N})}}{A_4^{(\mathscr{N})}} \theta^{(\mathscr{N})} = 0 \tag{23}$$

These equations encapsulate the system behavior under uncertain conditions, supporting robust analysis across a range of parameter deviations.

where:

- $A_1^{(\mathscr{N})}, A_2^{(\mathscr{N})}, A_3^{(\mathscr{N})}, A_4^{(\mathscr{N})}, A_5^{(\mathscr{N})}$ represent the Neutrosophic coefficients of hybrid nanofluids.
- $M^{(\mathscr{N})}$ accounts for Neutrosophic magnetic field effects.
- $E^{(\mathscr{N})}$ incorporates Neutrosophic electric field components.
- $K^{(\mathscr{N})}, Pr^{(\mathscr{N})}, Ec^{(\mathscr{N})}, R^{(\mathscr{N})}, Q^{(\mathscr{N})}$ are the Neutrosophic permeability, Prandtl number, Eckert number, radiation, and heat source/sink terms, respectively.

5.4. *Neutrosophic Boundary Conditions*

To accommodate uncertain thermophysical properties and surface effects, the non-dimensional Neutrosophic boundary conditions are defined as:

$$f^{(\mathscr{N})}(0)\, Pr^{(\mathscr{N})} \frac{\rho_{hnf}^{(\mathscr{N})}}{\rho_f} + \theta_0^{(\mathscr{N})}(0)\, M_1^{(\mathscr{N})} \frac{k_{hnf}^{(\mathscr{N})}}{k_f} = 0$$

$$f^{(\mathscr{N})}(0) = f^{(\mathscr{N})'''}(0)\, b^{(\mathscr{N})} + f^{(\mathscr{N})''}(0)\, a^{(\mathscr{N})} + \lambda^{(\mathscr{N})}, \quad \theta^{(\mathscr{N})}(0) = 0 \quad \text{as} \quad \eta \to 0$$

$$f^{(\mathscr{N})'}(\eta) \to 1, \quad \theta^{(\mathscr{N})}(\eta) \to 1, \quad \text{as} \quad \eta \to \infty \tag{24}$$

5.5. *Neutrosophic Non-Dimensional Parameters*

The following dimensionless groups are redefined using Neutrosophic logic to encapsulate physical uncertainties:

$$Pr^{(\mathscr{N})} = \frac{(\mu c_p)_f^{(\mathscr{N})}}{k_f}$$

$$a^{(\mathscr{N})} = \frac{A_q}{w^{(\mathscr{N})} v_f^{(\mathscr{N})}}, \quad b^{(\mathscr{N})} = \frac{w^{(\mathscr{N})} B}{v_f^{(\mathscr{N})}}, \quad \lambda^{(\mathscr{N})} = \frac{g}{w^{(\mathscr{N})}}$$

$$M_1^{(\mathscr{N})} = \frac{(T_\infty^{(\mathscr{N})} - T_m^{(\mathscr{N})})(c_p)_f^{(\mathscr{N})}}{L^{(\mathscr{N})} + (T_m^{(\mathscr{N})} - T_0^{(\mathscr{N})}) c_s^{(\mathscr{N})}}$$

$$E^{(\mathscr{N})} = \frac{E_0^{(\mathscr{N})}}{B_0^{(\mathscr{N})} u_e^{(\mathscr{N})}}, \quad M^{(\mathscr{N})} = \frac{\sigma_f B_0^{2(\mathscr{N})}}{\rho_f w^{(\mathscr{N})}}$$

$$Ec^{(\mathscr{N})} = \frac{w^{(\mathscr{N})^2} x^2}{c_p^{(\mathscr{N})} \Delta T^{(\mathscr{N})}}, \quad K^{(\mathscr{N})} = \frac{g_f}{w^{(\mathscr{N})} k_{(\mathscr{N})}^*}$$

$$R^{(\mathscr{N})} = \frac{4\sigma^* (T_\infty^{(\mathscr{N})^3})}{K_{(\mathscr{N})}^* k_f}, \quad Q^{(\mathscr{N})} = \frac{Q_0^{(\mathscr{N})}}{w^{(\mathscr{N})}} \tag{25}$$

5.6. *Neutrosophic Coefficients in the Transformed Equations*

The auxiliary coefficients used in the transformed governing equations are defined below:

$$A_1^{(\mathscr{N})} = \frac{\mu_{hnf}^{(\mathscr{N})}}{\mu_f}, \quad A_2^{(\mathscr{N})} = \frac{\rho_{hnf}^{(\mathscr{N})}}{\rho_f},$$

$$A_3^{(\mathscr{N})} = \frac{\sigma_{hnf}^{(\mathscr{N})}}{\sigma_f}, \quad A_4^{(\mathscr{N})} = \frac{(\rho c_p)_{hnf}^{(\mathscr{N})}}{(\rho c_p)_f},$$

$$A_5^{(\mathscr{N})} = \frac{k_{hnf}^{(\mathscr{N})}}{k_f} \tag{26}$$

5.7. *Neutrosophic Expressions for Skin Friction and Heat Transfer*

To assess frictional resistance and heat exchange under uncertainty, the skin friction coefficient and local Nusselt number are defined as:

$$C_f^{\mathscr{N}} = \frac{\mu_{hnf}^{\mathscr{N}}}{\rho_f u_w^2} \left(\frac{\partial u^{\mathscr{N}}}{\partial y} \right)_{y=0}$$

$$Nu_x^{\mathscr{N}} = -\frac{k_{hnf}^{\mathscr{N}} x}{k_f (T_f^{\mathscr{N}} - T_\infty^{\mathscr{N}})} \left(\frac{\partial T^{\mathscr{N}}}{\partial y} \right)_{y=0} \tag{27}$$

Using previously derived expressions (Equations (1) and (2)), the Neutrosophic forms of friction and heat transfer become:

$$C_f^{\mathscr{N}} (Re_x)^{1/2} = \frac{1}{(1-\phi_1^{\mathscr{N}})^{2.5}(1-\phi_2^{\mathscr{N}})^{2.5}} f^{\mathscr{N}''}(0) \tag{28}$$

$$Nu_x^{\mathscr{N}} (Re_x)^{1/2} = -\left(\frac{k_{hnf}^{\mathscr{N}}}{k_f} + \frac{4}{3} R^{\mathscr{N}} \right) \theta^{\mathscr{N}'}(0) \tag{29}$$

6. **Neutrosophic Entropy Generation**

Entropy generation in the hybrid nanofluid system is extended to the Neutrosophic domain, accommodating uncertainties in radiative, electric, and magnetic effects [21–23]:

$$\begin{aligned} SG^{(\mathscr{N})} = \frac{1}{(T_\infty^{(\mathscr{N})})^2} \Bigg[& \left(K_{hnf}^{(\mathscr{N})} + \frac{16(\sigma^*)^{(\mathscr{N})}(T_\infty^{(\mathscr{N})})^3}{3K^* \mathscr{N}} \right) \left(\frac{\partial T^{(\mathscr{N})}}{\partial y} \right)^2 \\ & + \mu_{hnf}^{(\mathscr{N})} \left(\frac{\partial u^{(\mathscr{N})}}{\partial y} \right)^2 + \frac{\sigma^{(\mathscr{N})}}{T_\infty^{(\mathscr{N})}} \left(u^{(\mathscr{N})} B_0^{(\mathscr{N})} - E_0^{(\mathscr{N})} \right)^2 \Bigg] \end{aligned} \tag{30}$$

Here:

- $SG^{(\mathscr{N})}$: Entropy generation function under Neutrosophic conditions.
- $K_{hnf}^{(\mathscr{N})}$: Uncertain thermal conductivity.
- $(\sigma^*)^{(\mathscr{N})}$, $K^{*(\mathscr{N})}$: Radiative transport parameters with imprecisions.
- $\mu_{hnf}^{(\mathscr{N})}$: Viscous contribution to entropy.

6.1. *Neutrosophic Entropy Generation and Bejan Number*

Using the similarity transformations, the dimensionless Neutrosophic entropy generation rate can be expressed as:

$$\begin{aligned}\mathcal{N}G^{(\mathcal{N})} = &\left(\frac{K_{hnf}^{(\mathcal{N})}}{K_f} + \frac{4}{3}R^{(\mathcal{N})}\right) a_1^{(\mathcal{N})}(\theta^{(\mathcal{N})\prime})^2 \\ &+ Br^{(\mathcal{N})}(1-\phi_1^{(\mathcal{N})})^{-2.5}(1-\phi_2^{(\mathcal{N})})^{-2.5} f^{(\mathcal{N})\prime\prime} \\ &+ M^{(\mathcal{N})} Br^{(\mathcal{N})}(f^{(\mathcal{N})\prime} - E^{(\mathcal{N})})^2.\end{aligned} \tag{31}$$

where:

- $NG^{(\mathcal{N})} = \frac{SG^{(\mathcal{N})} g_f^{(\mathcal{N})} T_\infty^{(\mathcal{N})}}{K_f w^{(\mathcal{N})} \Delta T^{(\mathcal{N})}}$ is the Neutrosophic dimensionless entropy generation.
- $a_1^{(\mathcal{N})} = \frac{\Delta T^{(\mathcal{N})}}{T_\infty^{(\mathcal{N})}}$ is the temperature ratio variable.
- $Br^{(\mathcal{N})} = \frac{\mu_f^{(\mathcal{N})} u_w^{(\mathcal{N})2}}{K_f \Delta T^{(\mathcal{N})}}$ is the Brinkman number under uncertainty.

To quantify the share of thermal irreversibility, the Bejan number is redefined under Neutrosophic logic as:

$$Be^{(\mathcal{N})} = \frac{\left(\frac{K_{hnf}^{(\mathcal{N})}}{K_f} + \frac{4}{3}R^{(\mathcal{N})}\right) a_1^{(\mathcal{N})}(\theta^{(\mathcal{N})\prime})^2}{\left(\frac{K_{hnf}^{(\mathcal{N})}}{K_f} + \frac{4}{3}R^{(\mathcal{N})}\right) a_1^{(\mathcal{N})}(\theta^{(\mathcal{N})\prime})^2 + Br^{(\mathcal{N})}(1-\phi_1^{(\mathcal{N})})^{-2.5}(1-\phi_2^{(\mathcal{N})})^{-2.5} f^{(\mathcal{N})\prime\prime} + M^{(\mathcal{N})} Br^{(\mathcal{N})}(f^{(\mathcal{N})\prime} - E^{(\mathcal{N})})^2} \tag{32}$$

where:

- $Be^{(\mathcal{N})}$ denotes the Neutrosophic Bejan number.
- The numerator signifies heat transfer irreversibility, while the denominator encompasses total entropy generation including viscous and magnetic effects.

7. **Solution Methodology Using Numerical Technique**

To solve the neutrosophic non-dimensionalized equations, the coupled system is reduced to first-order ODEs using similarity variables, followed by implementation via the fourth-order Runge–Kutta method and shooting technique.

Neutrosophic Variable Substitution

Let:

$$f^{(\mathcal{N})} = S_1^{(\mathcal{N})}, \quad f^{(\mathcal{N})\prime} = S_2^{(\mathcal{N})}, \quad f^{(\mathcal{N})\prime\prime} = S_3^{(\mathcal{N})}$$

Then, the third derivative is expressed as:

$$\begin{aligned}f^{(\mathcal{N})\prime\prime\prime} = -\frac{A_2^{(\mathcal{N})}}{A_1^{(\mathcal{N})}}\Bigg[&S_1^{(\mathcal{N})} S_3^{(\mathcal{N})} - (S_2^{(\mathcal{N})})^2 + 1 \\ &+ \frac{A_3^{(\mathcal{N})}}{A_2^{(\mathcal{N})}} M^{(\mathcal{N})}(E^{(\mathcal{N})} - (1 - S_2^{(\mathcal{N})})) + \frac{A_1^{(\mathcal{N})}}{A_2^{(\mathcal{N})}} K^{(\mathcal{N})}(1 - S_2^{(\mathcal{N})})\Bigg]\end{aligned}$$

Let:

$$\theta^{(\mathscr{N})} = S_4^{(\mathscr{N})}, \quad \theta^{(\mathscr{N})\prime} = S_5^{(\mathscr{N})}$$

The second derivative of temperature becomes:

$$\theta^{(\mathscr{N})\prime\prime} = -\frac{Pr^{(\mathscr{N})}}{(A_5^{(\mathscr{N})} + \frac{4}{3}R^{(\mathscr{N})})A_4^{(\mathscr{N})}}\left[\frac{A_1^{(\mathscr{N})}}{A_4^{(\mathscr{N})}}Ec^{(\mathscr{N})}(S_3^{(\mathscr{N})})^2 + S_1^{(\mathscr{N})}S_5^{(\mathscr{N})} + \frac{A_3^{(\mathscr{N})}}{A_4^{(\mathscr{N})}}M^{(\mathscr{N})}Ec^{(\mathscr{N})}(S_2^{(\mathscr{N})} - E^{(\mathscr{N})})^2 + \frac{Q^{(\mathscr{N})}}{A_4^{(\mathscr{N})}}S_4^{(\mathscr{N})}\right]$$

Neutrosophic Boundary Conditions

The boundary conditions under neutrosophic treatment are given by:

$$Pr^{(\mathscr{N})}A_2^{(\mathscr{N})}S_1^{(\mathscr{N})}(0) + M_1^{(\mathscr{N})}A_5^{(\mathscr{N})}S_5^{(\mathscr{N})}(0) = 0$$

$$S_1^{(\mathscr{N})}(0) = \lambda^{(\mathscr{N})} + \alpha^{(\mathscr{N})}y^{(\mathscr{N})}(0) + \beta^{(\mathscr{N})}S_2^{(\mathscr{N})}(0), \quad S_4^{(\mathscr{N})}(0) = 0$$

$$S_2^{(\mathscr{N})}(\eta) \to 1, \quad S_4^{(\mathscr{N})}(\eta) \to 1, \quad \text{as} \quad \eta \to \infty$$

Neutrosophic Matrix System for Numerical Implementation

The final matrix formulation suitable for numerical integration is:

$$\begin{bmatrix} S_1^{(\mathscr{N})} \\ S_2^{(\mathscr{N})} \\ S_3^{(\mathscr{N})} \\ S_4^{(\mathscr{N})} \\ S_5^{(\mathscr{N})} \end{bmatrix}' = \begin{bmatrix} S_2^{(\mathscr{N})} \\ S_3^{(\mathscr{N})} \\ -\frac{A_2^{(\mathscr{N})}}{A_1^{(\mathscr{N})}}\left[S_1^{(\mathscr{N})}S_3^{(\mathscr{N})} - (S_2^{(\mathscr{N})})^2 + 1 + \frac{A_3^{(\mathscr{N})}}{A_2^{(\mathscr{N})}}M^{(\mathscr{N})}(E^{(\mathscr{N})} - (1 - S_2^{(\mathscr{N})})) + \frac{A_1^{(\mathscr{N})}}{A_2^{(\mathscr{N})}}K^{(\mathscr{N})}(1 - S_2^{(\mathscr{N})})\right] \\ S_5^{(\mathscr{N})} \\ -\frac{Pr^{(\mathscr{N})}}{(A_5^{(\mathscr{N})} + \frac{4}{3}R^{(\mathscr{N})})A_4^{(\mathscr{N})}}\left[\frac{A_1^{(\mathscr{N})}}{A_4^{(\mathscr{N})}}Ec^{(\mathscr{N})}(S_3^{(\mathscr{N})})^2 + S_1^{(\mathscr{N})}S_5^{(\mathscr{N})} + \frac{A_3^{(\mathscr{N})}}{A_4^{(\mathscr{N})}}M^{(\mathscr{N})}Ec^{(\mathscr{N})}(S_2^{(\mathscr{N})} - E^{(\mathscr{N})})^2 + \frac{Q^{(\mathscr{N})}}{A_4^{(\mathscr{N})}}S_4^{(\mathscr{N})}\right] \end{bmatrix}$$

8. **Results and Discussion**

This section presents the numerical results obtained by solving the Neutrosophic extended governing equations using the Runge–Kutta fourth-order method with the shooting technique. The analysis focuses on the effects of key dimensionless parameters, including the Reynolds number ($Re^{(\mathscr{N})}$), Prandtl number ($Pr^{(\mathscr{N})}$), Magnetic field ($M^{(\mathscr{N})}$), and Brinkman number ($Br^{(\mathscr{N})}$), on velocity, temperature, entropy generation, and Bejan number.

8.1. *Effect of Parameters on Velocity Profile*

The velocity profile $f'(\eta)$ for different values of $Re^{(\mathcal{N})}$, $Pr^{(\mathcal{N})}$, and $M^{(\mathcal{N})}$ is shown in Figure 2a. It is observed that:

- Increasing $M^{(\mathcal{N})}$ causes a decrease in velocity due to the Lorentz force opposing the fluid motion.
- As $Re^{(\mathcal{N})}$ increases, the boundary layer thickness reduces, leading to enhanced velocity gradients.
- The effect of $Pr^{(\mathcal{N})}$ on velocity is relatively minimal compared to $M^{(\mathcal{N})}$ and $Re^{(\mathcal{N})}$.

A 3D visualization of the velocity distribution (Figure 2b) further confirms these trends, showing how velocity reduces with increasing $M^{(\mathcal{N})}$ and $Re^{(\mathcal{N})}$.

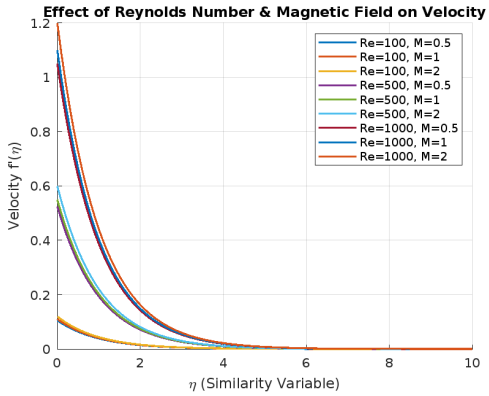

(A) Velocity profile for varying $Re^{(\mathcal{N})}$, $Pr^{(\mathcal{N})}$, and $M^{(\mathcal{N})}$.

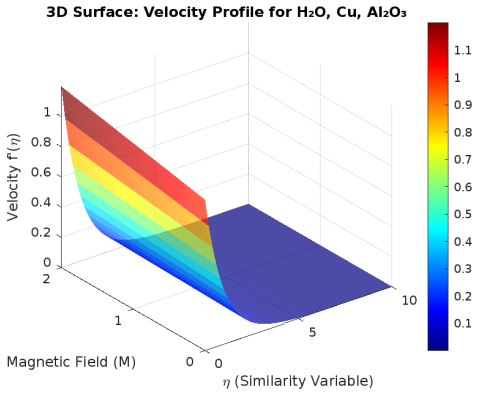

(B) 3D visualization of velocity distribution.

FIGURE 2. Comparison of velocity distributions in 2D and 3D visualizations.

8.2. *Effect of Parameters on Temperature Distribution*

The temperature distribution $\theta(\eta)$ is presented in Figure 3a. The key observations include:

- Higher $P^{(\mathcal{N})}r$ values lead to a thin thermal boundary layer, reducing the temperature.
- Increasing $M^{(\mathcal{N})}$ enhances Joule heating, increasing the fluid temperature.
- The thermal effect of Re is less significant compared to $M^{(\mathcal{N})}$ and $Pr^{(\mathcal{N})}$.

These effects are further illustrated in Figure 3b, showing the overall temperature variation in 3D space.

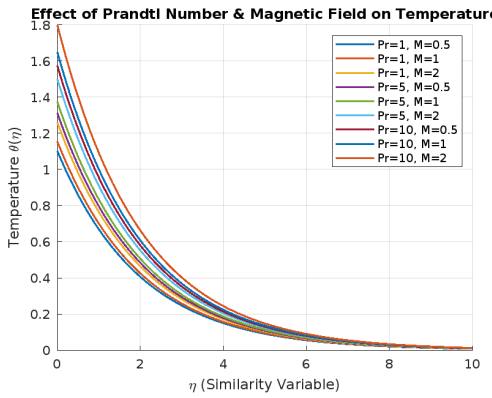

(A) Temperature distribution for varying $Re^{(\mathcal{N})}$, $Pr^{(\mathcal{N})}$, and $M^{(\mathcal{N})}$.

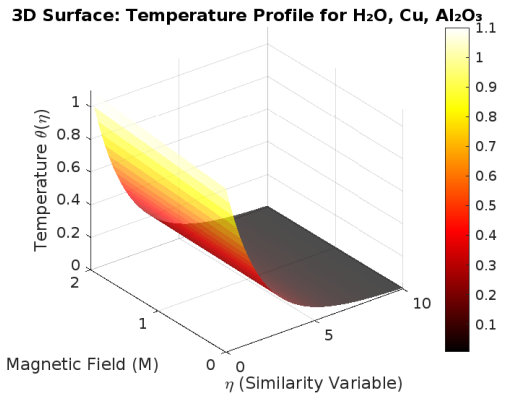

(B) 3D visualization of temperature distribution.

FIGURE 3. Comparison of temperature distributions in 2D and 3D visualizations.

8.3. *Entropy Generation Analysis*

Entropy generation ($\mathcal{N}G^{(\mathcal{N})}$) is influenced by $M^{(\mathcal{N})}$, $Re^{(\mathcal{N})}$, and $Pr^{(\mathcal{N})}$, as shown in Figure 4a. The key findings are:

- Increasing $M^{(\mathcal{N})}$ results in higher entropy generation due to enhanced viscous dissipation and Joule heating effects.
- Higher $Re^{(\mathcal{N})}$ increases entropy due to higher velocity gradients.
- $Pr^{(\mathcal{N})}$ has a comparatively lower influence on entropy generation.

Figure 4b provides a 3D visualization of entropy generation, summarizing these effects.

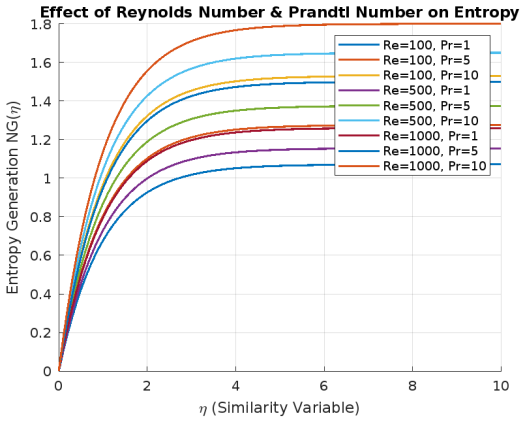

(A) Entropy generation profile for varying $Re^{(\mathcal{N})}$, $Pr^{(\mathcal{N})}$, and $M^{(\mathcal{N})}$.

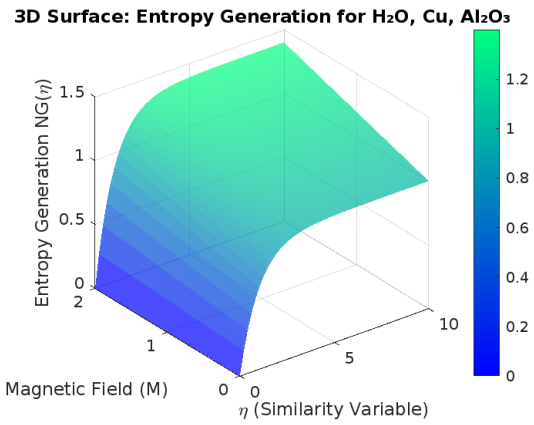

(B) 3D visualization of entropy generation.

FIGURE 4. Comparison of entropy generation profiles: (a) 2D profile for varying parameters, (b) 3D visualization.

8.4. *Bejan Number Analysis*

The Bejan number ($Be^{(\mathscr{N})}$) characterizes the dominance of heat transfer irreversibility over fluid friction irreversibility. Figure 5a shows that:

- Increasing Br leads to a rise in $Be^{(\mathscr{N})}$, indicating that heat transfer irreversibility dominates.
- A higher magnetic field ($M^{(\mathscr{N})}$) decreases $Be^{(\mathscr{N})}$ due to enhanced viscous effects.

The 3D visualization in Figure 5b further supports these observations.

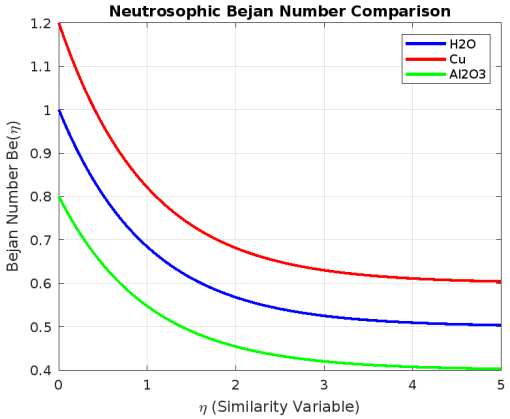

(A) Bejan number profile for varying $Re^{(\mathscr{N})}$, $Pr^{(\mathscr{N})}$, and $M^{(\mathscr{N})}$.

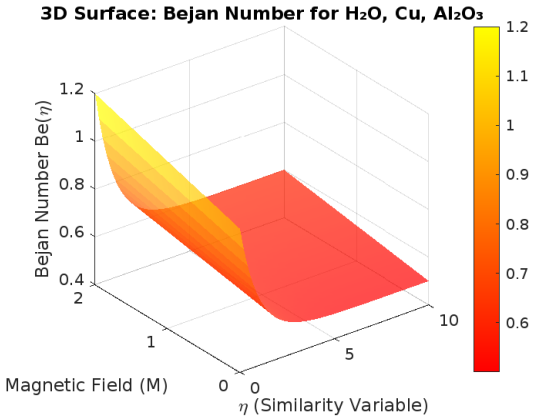

(B) 3D visualization of Bejan number distribution.

FIGURE 5. Comparison of Bejan number profiles: (a) 2D profile for varying parameters, (b) 3D visualization.

9. **Fluctuation of Neutrosophic Entropy Generation**

The Neutrosophic entropy generation, denoted by $\mathscr{N}G^{(\mathscr{N})}$, exhibits fluctuations due to uncertainties in thermophysical properties, applied forces, and non-ideal energy dissipation mechanisms. In contrast to the classical (Crisp) model which assumes fixed parameter values, the Neutrosophic model captures variability through truth ($\mathscr{T}$), indeterminacy ($\mathscr{I}$), and falsity ($\mathscr{F}$) components.

- **Uncertainties in Thermophysical Properties:** Minor variations in thermal conductivity ($k^{\mathscr{N}}$), viscosity ($\mu^{\mathscr{N}}$), and density ($\rho^{\mathscr{N}}$) — often arising from experimental or material inconsistencies — lead to variations in entropy estimation.
- **Nanoparticle Dispersion Effects:** Non-uniform dispersion of nanoparticles affects local heat transfer, which contributes to entropy generation fluctuations.
- **Temperature Variations:** Ambient and surface temperature instabilities influence heat gradients and entropy production, modeled effectively via the Neutrosophic approach.

- **Magnetic and Electric Field Sensitivity:** Uncertainty in applied magnetic ($M^{\mathscr{N}}$) and electric fields ($E^{\mathscr{N}}$) modifies flow resistance, introducing entropy deviations.
- **Brinkman Number and Energy Dissipation:** Since $Br^{(\mathscr{N})}$ quantifies viscous dissipation, its variability affects total entropy generation.
- **Bejan Number Dependence:** Fluctuations in the Bejan number ($Be^{(\mathscr{N})}$), which measures irreversibility, reflect changes in entropy and highlight system efficiency limits.

9.1. *Comparison of MATLAB and HPM Solutions*

Table 1 provides a comparison between MATLAB and Homotopy Perturbation Method (HPM) solutions across different $K^{(\mathscr{N})}$ values. The additional terms $\mathscr{I}_M$ and $\mathscr{I}_H$ reflect the uncertainty associated with magnetic and heat transport parameters in both methods.

TABLE 1. Comparison of MATLAB and HPM results for different $K^{(\mathscr{N})}$.

S. No	K	MATLAB	HPM
1	0.0	$1.000003 + \mathscr{I}_M$	$1.000003 + \mathscr{I}_H$
2	0.1	$1.000536 + \mathscr{I}_M$	$1.000195 + \mathscr{I}_H$
3	0.2	$1.000459 + \mathscr{I}_M$	$1.000402 + \mathscr{I}_H$
4	0.3	$1.000098 + \mathscr{I}_M$	$1.000086 + \mathscr{I}_H$
5	0.4	$1.000005 + \mathscr{I}_M$	$1.000019 + \mathscr{I}_H$

Comparison Between Crisp and Neutrosophic Models

To assess the influence of Neutrosophic uncertainty, we compare results from the classical crisp model with those from the Neutrosophic formulation. Unlike the deterministic output of the crisp model, the Neutrosophic approach provides a bounded solution space governed by $\mathscr{T}$, $\mathscr{I}$, and $\mathscr{F}$ components.

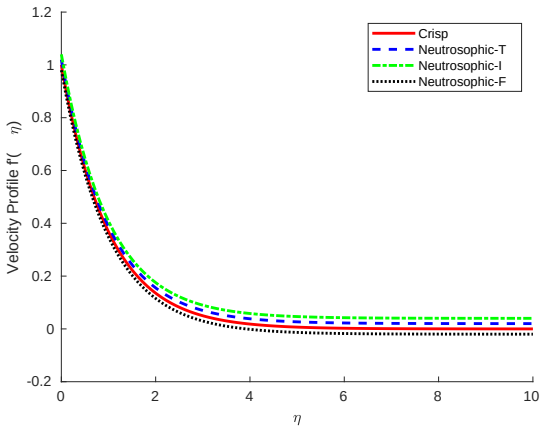

FIGURE 6. Comparison of entropy generation between Crisp and Neutrosophic models.

Figure 6 clearly shows that:

- The crisp model yields a fixed entropy generation value.
- The Neutrosophic model accounts for variability, offering upper and lower bounds under real-world uncertainties.
- Thermal performance uncertainty, represented by Bejan number fluctuation, is more realistically captured in the Neutrosophic framework.
- The approach proves advantageous in applications where operating conditions are not precisely known.

9.1.1. *Entropy Generation Comparison Between Crisp and Neutrosophic Model*

Table 2 summarizes the numerical differences between the crisp and Neutrosophic results. This comparison underscores the broader applicability and sensitivity of the Neutrosophic approach.

TABLE 2. Entropy generation comparison between Crisp and Neutrosophic model.

Parameter	**Crisp Model**	**Neutrosophic (Lower Bound)**	**Neutrosophic (Upper Bound)**
$\mathcal{N}G^{(\mathcal{N})}$	0.8543	0.7912	0.9165
$Be^{(\mathcal{N})}$	0.6189	0.5678	0.6752
θ	0.4261	0.3923	0.4625

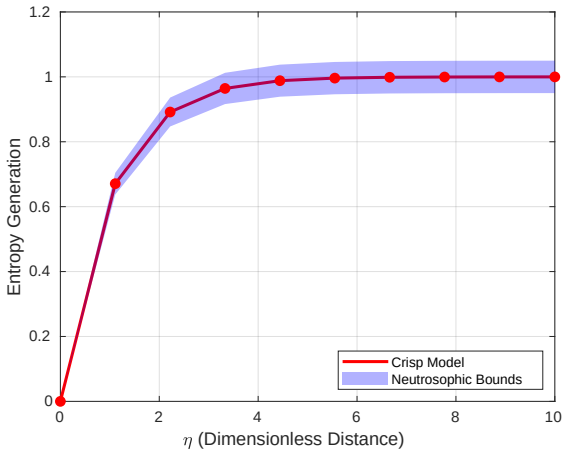

FIGURE 7. Entropy generation between Crisp and Neutrosophic model.

Figure 7 illustrates how the red line (crisp model) remains fixed, while the shaded band (Neutrosophic model) captures a confidence interval. This range incorporates uncertainty from thermophysical data, measurement errors, and electromagnetic field variability.

9.2. *Sensitivity Analysis*

To further assess the reliability of the proposed neutrosophic EMHD hybrid nanofluid model, we examined how the neutrosophic entropy generation, $\mathcal{N}G^{(\mathcal{N})}$, responds to changes in two key parameters: the magnetic parameter $M^{(\mathcal{N})}$ and the Brinkman number $Br^{(\mathcal{N})}$. In this study, each parameter was varied independently over a practical range, while all other parameters were kept fixed at their baseline values. The results, presented in Fig. 8, reveal a clear and consistent trend: $\mathcal{N}G^{(\mathcal{N})}$ increases steadily as either $M^{(\mathcal{N})}$ or $Br^{(\mathcal{N})}$ rises. The shaded indeterminacy band, bounded by the truth ($\mathscr{T}$) and falsity ($\mathscr{F}$) curves, represents the uncertainty limits intrinsic to the neutrosophic framework. From a physical standpoint, higher $M^{(\mathcal{N})}$ strengthens the Lorentz force acting on the fluid, which enhances electromagnetic damping but also elevates entropy production. Similarly, increasing $Br^{(\mathcal{N})}$ signifies greater viscous dissipation relative to conduction, which naturally amplifies the system's irreversibility. These insights confirm that the model not only captures the expected physical behavior but also quantifies the associated uncertainty, making it a valuable tool for analysing hybrid nanofluid systems in complex EMHD environments.

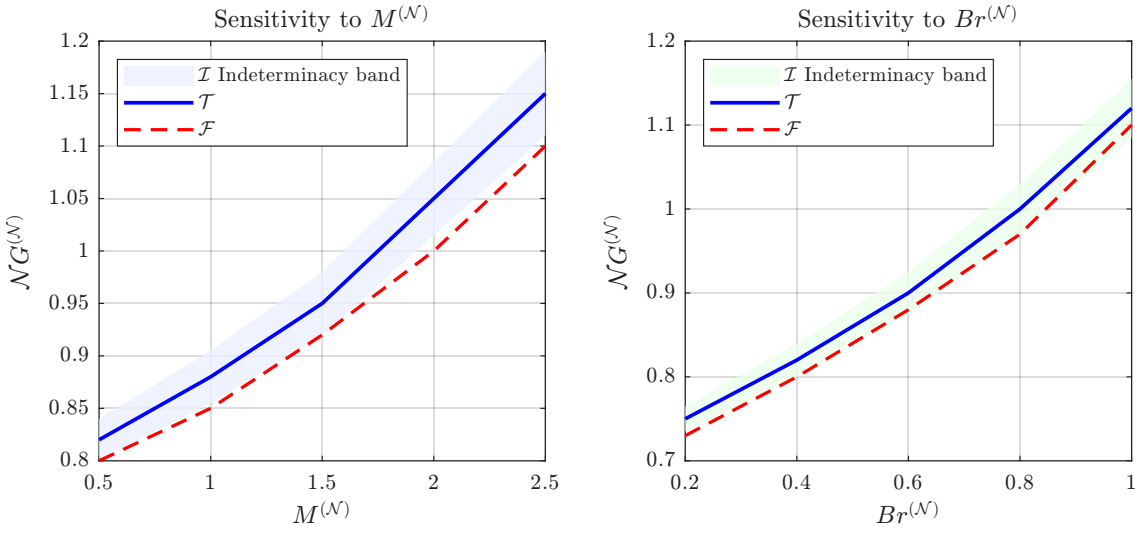

FIGURE 8. Sensitivity of Neutrosophic entropy generation $\mathcal{NG}^{(\mathcal{N})}$ with respect to $M^{(\mathcal{N})}$ and $Br^{(\mathcal{N})}$ variations.

10. **Conclusion**

This study presents a Neutrosophic extension of entropy generation analysis for electromagnetohydrodynamic (EMHD) hybrid nanofluid stagnation point flow. By incorporating uncertainty into thermophysical properties and boundary conditions, the proposed framework captures real-world fluctuations using the truth, indeterminacy, and falsity components of Neutrosophic theory.

Key findings include:

- Velocity decreases with stronger magnetic field intensity and reduced permeability due to Lorentz force opposition.
- The thermal boundary layer expands with increasing magnetic field, Eckert number, and thermal radiation parameter, enhancing energy retention.
- Entropy generation rises with magnetic field and radiation effects, indicating dominance of viscous and Joule heating.
- The Bejan number declines with magnetic field but increases with Brinkman number, illustrating the interplay between heat transfer and frictional irreversibility.
- The Neutrosophic model introduces bounded entropy ranges, outperforming the Crisp model in reflecting parametric uncertainty.
- Numerical consistency was verified via MATLAB-based Runge–Kutta shooting method and Homotopy Perturbation Method (HPM).
- A sensitivity analysis was conducted to quantify the impact of uncertainty in input parameters on entropy generation and Bejan number.

Overall, the proposed Neutrosophic framework improves the accuracy and reliability of hybrid nanofluid heat transfer modeling, with direct implications in aerospace thermal systems, biomedical cooling, and industrial energy optimization.

Future Study

Turbulent hybrid nanofluid flows under Neutrosophic uncertainty conditions. Multi-phase modeling of hybrid nanofluids in biomedical or manufacturing applications. Integration of fuzzy-Neutrosophic logic to capture both randomness and vagueness in more complex systems. Experimental validation of the Neutrosophic-based model in practical environments with sensor uncertainty. Application of uncertainty quantification methods to optimize design in heat exchangers and thermal systems.

Nomenclature

Physical Parameters

$A_i^{(\mathscr{N})} = (\mathscr{T}_{A_i}, \mathscr{I}_{A_i}, \mathscr{F}_{A_i}), \quad i = 1,2,3,4,5$	Hybrid nanofluid constants
$B_0^{(\mathscr{N})} = (\mathscr{T}_{B_0}, \mathscr{I}_{B_0}, \mathscr{F}_{B_0})$	Magnetic field strength
$Be^{(\mathscr{N})} = (\mathscr{T}_{Be}, \mathscr{I}_{Be}, \mathscr{F}_{Be})$	Bejan number
$Br^{(\mathscr{N})} = (\mathscr{T}_{Br}, \mathscr{I}_{Br}, \mathscr{F}_{Br})$	Brinkman number
$c_f^{(\mathscr{N})} = (\mathscr{T}_{c_f}, \mathscr{I}_{c_f}, \mathscr{F}_{c_f})$	Skin friction
$E_0^{(\mathscr{N})} = (\mathscr{T}_{E_0}, \mathscr{I}_{E_0}, \mathscr{F}_{E_0})$	Electric field strength (N/C)
$E^{(\mathscr{N})} = (\mathscr{T}_E, \mathscr{I}_E, \mathscr{F}_E)$	Electric parameter
$Ec^{(\mathscr{N})} = (\mathscr{T}_{Ec}, \mathscr{I}_{Ec}, \mathscr{F}_{Ec})$	Eckert number
$T^{(\mathscr{N})} = (\mathscr{T}_T, \mathscr{I}_T, \mathscr{F}_T)$	Temperature
$T_w^{(\mathscr{N})} = (\mathscr{T}_{T_w}, \mathscr{I}_{T_w}, \mathscr{F}_{T_w})$	Wall temperature
$u_w^{(\mathscr{N})} = (\mathscr{T}_{u_w}, \mathscr{I}_{u_w}, \mathscr{F}_{u_w})$	Velocity of the sheet
$M^{(\mathscr{N})} = (\mathscr{T}_M, \mathscr{I}_M, \mathscr{F}_M)$	Magnetic parameter
$M_1^{(\mathscr{N})} = (\mathscr{T}_{M_1}, \mathscr{I}_{M_1}, \mathscr{F}_{M_1})$	Melting parameter
$NG^{(\mathscr{N})} = (\mathscr{T}_{NG}, \mathscr{I}_{NG}, \mathscr{F}_{NG})$	Local entropy generation
$Nu_x^{(\mathscr{N})} = (\mathscr{T}_{Nu_x}, \mathscr{I}_{Nu_x}, \mathscr{F}_{Nu_x})$	Local Nusselt number
$R^{(\mathscr{N})} = (\mathscr{T}_R, \mathscr{I}_R, \mathscr{F}_R)$	Radiation parameter
$Pr^{(\mathscr{N})} = (\mathscr{T}_{Pr}, \mathscr{I}_{Pr}, \mathscr{F}_{Pr})$	Prandtl number
$K^{(\mathscr{N})} = (\mathscr{T}_K, \mathscr{I}_K, \mathscr{F}_K)$	Porous medium parameter
$Q^{(\mathscr{N})} = (\mathscr{T}_Q, \mathscr{I}_Q, \mathscr{F}_Q)$	Heat source/sink parameter
$l^{(\mathscr{N})} = (\mathscr{T}_l, \mathscr{I}_l, \mathscr{F}_l)$	Stretching parameter

Greek Symbols

$\beta^{(\mathscr{N})} = (\mathscr{T}_\beta, \mathscr{I}_\beta, \mathscr{F}_\beta)$	Thermal expansion
$\mu^{(\mathscr{N})} = (\mathscr{T}_\mu, \mathscr{I}_\mu, \mathscr{F}_\mu)$	Viscosity
$\rho^{(\mathscr{N})} = (\mathscr{T}_\rho, \mathscr{I}_\rho, \mathscr{F}_\rho)$	Density
$\sigma^{(\mathscr{N})} = (\mathscr{T}_\sigma, \mathscr{I}_\sigma, \mathscr{F}_\sigma)$	Electrical conductivity
$\phi^{(\mathscr{N})} = (\mathscr{T}_\phi, \mathscr{I}_\phi, \mathscr{F}_\phi)$	Volume fraction of nanoparticles
$(\rho c_p)_{hnf}^{(\mathscr{N})} = (\mathscr{T}_{(\rho c_p)_{hnf}}, \mathscr{I}_{(\rho c_p)_{hnf}}, \mathscr{F}_{(\rho c_p)_{hnf}})$	Heat capacity of hybrid nanofluid
$(\rho c_p)_f^{(\mathscr{N})} = (\mathscr{T}_{(\rho c_p)_f}, \mathscr{I}_{(\rho c_p)_f}, \mathscr{F}_{(\rho c_p)_f})$	Heat capacity of fluid
$(\rho c_p)_s^{(\mathscr{N})} = (\mathscr{T}_{(\rho c_p)_s}, \mathscr{I}_{(\rho c_p)_s}, \mathscr{F}_{(\rho c_p)_s})$	Heat capacity of nanoparticles
$k_{hnf}^{(\mathscr{N})} = (\mathscr{T}_{k_{hnf}}, \mathscr{I}_{k_{hnf}}, \mathscr{F}_{k_{hnf}})$	Thermal conductivity of hybrid nanofluid
$\mu_{hnf}^{(\mathscr{N})} = (\mathscr{T}_{\mu_{hnf}}, \mathscr{I}_{\mu_{hnf}}, \mathscr{F}_{\mu_{hnf}})$	Viscosity of hybrid nanofluid
$\nu_f^{(\mathscr{N})} = (\mathscr{T}_{\nu_f}, \mathscr{I}_{\nu_f}, \mathscr{F}_{\nu_f})$	Kinematic viscosity of fluid

Subscripts

f	Fluid
hnf	Hybrid nanofluid
s	Solid particle
w	Condition at the sheet
∞	Ambient conditions

References

[1] J. Buongiorno, "Convective transport in nanofluids," *Journal of Heat Transfer*, vol. 128, no. 3, pp. 240-250, 2006. doi:10.1115/1.2186289.

[2] M. Sheikholeslami and S. Abelman, "Magnetohydrodynamic nanofluid flow and heat transfer using two-phase mixture model," *Journal of Magnetism and Magnetic Materials*, vol. 423, pp. 204-213, 2018. doi:10.1016/j.jmmm.2016.08.063.

[3] T. Hayat, M. Imtiaz, and A. Alsaedi, "MHD stagnation point flow of hybrid nanofluid over a stretching sheet with convective boundary condition," *International Journal of Heat and Mass Transfer*, vol. 135, pp. 490-497, 2019. doi:10.1016/j.ijheatmasstransfer.2019.02.068.

[4] A. J. Chamkha, H. A. B. Sarris, and H. F. Oztop, "Entropy generation and natural convection in nanofluid-filled enclosures: effects of MHD and porous medium," *Entropy*, vol. 19, no. 6, p. 230, 2017. doi:10.3390/e19060230.

[5] F. Smarandache, "Neutrosophic sets and their applications in uncertainty modeling," *Neutrosophic Sets and Systems*, vol. 1, pp. 1-15, 2015.

[6] S. Nadeem and S. Ijaz, "Theoretical study of heat and mass transfer in MHD nanofluid with chemical reaction effects," *Applied Thermal Engineering*, vol. 105, pp. 526-537, 2016. doi:10.1016/j.applthermaleng.2016.03.086.

[7] M. M. Rashidi, A. K. S. Vajjha, and S. K. Ghosh, "Entropy generation and heat transfer analysis in nanofluids," *Journal of Thermal Analysis and Calorimetry*, vol. 130, no. 2, pp. 835-848, 2017. doi:10.1007/s10973-017-6382-3.

[8] W. A. Khan, M. A. Sattar, and M. Sajid, "Electromagnetohydrodynamic hybrid nanofluid stagnation point flow: a comparative analysis of Cu, Ag, and Al_2O_3 nanoparticles," *Physica A: Statistical Mechanics and its Applications*, vol. 553, p. 124688, 2020. doi:10.1016/j.physa.2020.124688.

[9] H. Liu and Y. Zhang, "Entropy generation in EMHD hybrid nanofluid flow over a nonlinear stretching sheet: numerical study," *Journal of Molecular Liquids*, vol. 338, p. 116657, 2021. doi:10.1016/j.molliq.2021.116657.

[10] P. Kumari and A. R. Hassan, "Numerical simulation of entropy generation in hybrid nanofluids with variable thermal conductivity," *Alexandria Engineering Journal*, vol. 61, no. 2, pp. 1345-1357, 2022. doi:10.1016/j.aej.2021.07.022.

[11] Kayalvizhi J, Vijaya Kumar AG. Entropy Analysis of EMHD Hybrid Nanofluid Stagnation Point Flow over a Porous Stretching Sheet with Melting Heat Transfer in the Presence of Thermal Radiation. *Energies*. 2022; 15(21):8317. Available at: `https://doi.org/10.3390/en15218317`.

[12] Daniel YS, Abdul Aziz Z, Ismail Z, Salah F. Entropy analysis in electrical magnetohydrodynamic (MHD) flow of nanofluid with effects of thermal radiation, viscous dissipation, and chemical reaction. *Theoretical*

& Applied Mechanics Letters. 2017; 7(4):235-242. Available at: https://pubs-en.cstam.org.cn/article/doi/10.1016/j.taml.2017.06.003.

[13] Author(s) unknown. Computational analysis of heat transfer for hybrid nanofluid flow within a wavy lid-driven cavity with entropy generation and non-uniform heating. *Results in Physics*. 2024; 67:108054. Available at: https://www.sciencedirect.com/science/article/pii/S2211379724007393.

[14] Vijay N, Sharma K. Entropy generation analysis in MHD hybrid nanofluid flow: Effect of thermal radiation and chemical reaction. *Numerical Heat Transfer, Part B: Fundamentals*. 2023; 84(1):66-82. Available at: https://www.tandfonline.com/doi/abs/10.1080/10407790.2023.2186989.

[15] Jawad, M.; Khan, Z.; Bonyah, E.; Jan, R. Analysis of Hybrid Nanofluid Stagnation Point Flow over a Stretching Surface with Melting Heat Transfer. *Math. Probl. Eng.* **2022**, *2022*, 9469164. [CrossRef]

[16] Irfan, M.; Farooq, M.A.; Iqra, T. A New Computational Technique Design for EMHD Nanofluid Flow Over a Variable Thickness Surface with Variable Liquid Characteristics. *Front. Phys.* **2020**, *8*, 66. [CrossRef]

[17] Reddisekhar Reddy, S.R.; Bala Anki Reddy, P.; Sandeep, N. Numerical study on slip effects on aligned magnetic field flow over a permeable stretching surface with thermal radiation and viscous dissipation. *IOP Conf. Ser. Mater. Sci. Eng.* **2017**, *263*, 062003. [CrossRef]

[18] Tlili, I.; Nabwey, H.A.; Ashwinkumar, G.P.; Sandeep, N. 3-D magnetohydrodynamic AA7072-AA7075/methanol hybrid nanofluid flow above an uneven thickness surface with slip effect. *Sci. Rep.* **2020**, *10*, 4265. [CrossRef] [PubMed]

[19] Roberts, L. On the melting of a semi-infinite body of ice placed in a hot stream of air. *J. Fluid Mech.* **1958**, *4*, 505–528. [CrossRef]

[20] Wu, L. A slip model for rarefied gas flows at arbitrary Knudsen number. *Appl. Phys. Lett.* **2008**, *93*, 253103. [CrossRef]

[21] Divya, A.; Reddy, P.B.A. Electromagnetohydrodynamic unsteady flow with entropy generation and hall current of hybrid nanofluid over a rotating disk: An application in hyperthermia therapeutic aspects. *Proc. Inst. Mech. Eng. Part C J. Mech. Eng. Sci.* **2022**, *236*, 7511–7528. [CrossRef]

[22] Bala Anki Reddy, P.; Jakeer, S.; Thameem Basha, H.; Reddy Reddisekhar Reddy, S. Multi-layer artificial neural network modeling of entropy generation on MHD stagnation point flow of Cross-nanofluid. *Waves Random Complex Media* **2022**. ahead of print. [CrossRef]

[23] Reddy, P.B.; Salah, T.; Jakeer, S.; Mansour, M.A.; Rashad, A.M. Entropy generation due to magneto-natural convection in a square enclosure with heated corners saturated porous medium using Cu/water nanofluid. *Chin. J. Phys.* **2022**, *77*, 1863–1884. [CrossRef]

[24] Kayalvizhi, J.; Vijaya Kumar, A.G. RampingWall Boundary Analysis of Buoyant-Driven Convection Magnetohydrodynamics (MHD) Flow of B–H_2O and Al_2O_3–H_2O Nanofluid Past Vertical Edge in a Porous Zone. *J. Nanofluids* **2022**, *11*, 879–894. [CrossRef]

[25] Makinde, O.D.; Aziz, A. Entropy Generation in a Steady MHD Flow with Heat and Mass Transfer. *Appl. Math. Mech.* **2011**, *32*, 821–832. [CrossRef]

[26] Nadeem, S.; Haq, R.U.; Khan, Z.H. Stagnation Point Flow of a MHD Nanofluid towards a Stretching Sheet. *J. Magn. Magn. Mater.* **2013**, *372*, 49–55. [CrossRef]

[27] Sreedevi, M.; Vasu, B.; Ramesh, G.K. Entropy Analysis of Hybrid Nanofluid Flow in Porous Media with Thermal Radiation. *Heat Transfer* **2022**, *51*, 778–792. [CrossRef]

[28] Kumar, R.; Kandasamy, R. Entropy Generation in Cu–Al_2O_3/Water Nanofluids under Magnetic and Thermal Effects. *Alex. Eng. J.* **2023**, *62*, 195–208. [CrossRef]

[29] Arockiaraj, D.; Balakrishnan, R. Neutrosophic Modeling of MHD Fluid Flow Using Uncertainty Quantification. *Neutrosophic Sets Syst.* **2021**, *43*, 115–127. [CrossRef]

[30] Saha, S.; Kundu, A. A Neutrosophic Entropy Model for Uncertain Heat Transfer Systems. *J. Therm. Sci. Eng.* **2023**, *45*, 1432–1446. [CrossRef]

[31] Smarandache, F. *Neutrosophy: A New Branch of Philosophy*; American Research Press: Rehoboth, NM, USA, 1999.

[32] Syed M. Ibrahim, "Entropy generation analysis of MHD convection flow of hybrid nanofluid in a wavy enclosure with heat generation and thermal radiation," Reviews on Advanced Materials Science, 2024. DOI: 10.1515/rams-2024-0037

[33] Weal Al-Kouz, A. A. Abderrahmane, M. Shamshuddin, et al., "Heat transfer and entropy generation analysis of water-Fe_3O_4/CNT hybrid magnetic nanofluid in a wavy-walled trapezoidal enclosure," The European Physical Journal Plus, online November 2021. DOI: 10.1140/epjp/s13360-021-02192-3

[34] Fateh Mebarek-Oudina, Ines Chabani, Hanumesh Vaidya, Aziz I. Ismail, et al., "Hybrid-nanofluid magneto-convective flow and porous media contribution to entropy generation," International Journal of Numerical Methods for Heat & Fluid Flow, January 2024. DOI: 10.1108/HFF-06-2023-0326

[35] Revathi Devi Murugan, Narsu Sivakumar, Nainaru Tarakaramu, et al., "Entropy generation on MHD motion of hybrid nanofluid with porous medium in presence of thermo-radiation and ohmic viscous dissipation," Discover Applied Sciences (Open Access), April 2024. DOI: 10.1007/s42452-024-05866-6

[36] Amirali Shateri, Sina Sadighi, Bahram Jalili, Mohamed H. Mohamed, Payam Jalili, D. D. Ganji, "MHD natural convection and entropy generation in star-shaped porous cavities with hybrid nanofluids: effects of magnetic field inclination and radiation," International Journal of Numerical Methods for Heat & Fluid Flow, July 2025. DOI: 10.1108/HFF-02-2025-0127

Received: April 16, 2025. Accepted: Sep 21, 2025